Journal of
Nanoelectronics and Optoelectronics
Vol. 2, 209–221, 2007

REVIEW

Closing the Gap: Plasma Wave Electronic Terahertz Detectors

W. J. Stillman* and M. S. Shur

Center for Integrated Electronics, Rensselaer Polytechnic Institute, Troy, NY 12180, USA

The terahertz portion of the electromagnetic spectrum is experiencing a substantial growth in interest, with new applications in security, medicine and communications, among others, emerging at a rapid pace. Limitations in source power, the reported "terahertz gap," place stringent requirements upon THz detector device performance in terms of responsivity, sensitivity and response speed. In this paper, we review the present state-of-the-art in terahertz sources and detectors, and discuss in some detail the operation of an emerging class of plasma wave terahertz devices.

Keywords: Terahertz, Detectors, Sensors, Plasma Wave Electronics.

CONTENTS

1. INTRODUCTION

Originally of interest for astronomical science and earth observation, the terahertz portion of the electromagnetic spectrum has gained an ever increasing attention in recent years. Potential applications abound in communications, materials identification and imaging, the latter driven largely today by security concerns, where hidden hazardous agents may be detected. Applications in medical imaging, both external and internal[1] to the human body are also experiencing a substantial growth in interest. Examples of terahertz imaging applications are shown Figures 1–4 Present imaging techniques are divided between Pulsed Time Domain (PTD) and Continuous Wave (CW) modalities. PTD imaging affords a greater diversity of information, including depth, range and nature of scattering objects, including absorption spectra, while CW imaging information is typically limited to intensity, though depth and range may be discerned by increasing detection complexity.[2] PTD systems tend to be bulkier and more expensive than CW systems, and can be more difficult to set up. Imaging in PTD systems tends to be more involved than is the case for CW systems due to the complexity of the image data. In either system, imaging may be of the radiation transmitted through or reflected by the object.

As indicated in Figures 1 and 2, CW imaging systems can be passive, where the terahertz or sub-terahertz energy analyzed is present in the environment or emitted by the object itself (typically the human body), or active, where the energy is supplied by a dedicated source. In active systems, source power is of major concern, since it is at present very limited. For both active and passive systems, the terahertz detector plays a crucial role, and in this paper, we briefly review the state-of-the-art of existing terahertz detectors, and discuss emerging plasma wave electronic devices as detectors of terahertz radiation. In order to provide context for our discussions, we begin with a brief review of terahertz emitters.

2. TERAHERTZ EMITTERS

For security applications, likely beam power requirements are between 1 mW and 1 W (Ref. [3]), thus in addition to work on faster and more sensitive CW detectors, development of more powerful sources is essential. Irradiation power restrictions in medical imaging applications (1 mW/cm^2).[3] In this case, the maximum imaging depth due to attenuation of the terahertz signal is limited to ~1 mm. As with terahertz detectors, there are two modalities

*Author to whom correspondence should be addressed.

 1555-130X/2007/2/209/013 doi:10.1166/jno.2007.301

associated with terahertz sources. In Pulsed Time Domain (PTD) systems, terahertz radiation is typically generated by illumination of a photoconductive antenna with radiation from ultrafast gas or solid state lasers. A novel approach replaces the photoconductive antenna with a laser induced air plasma[4] which overcomes the atmospheric attenuation inherent in transmission of terahertz radiation across substantial distances. Terahertz sources capable of Continuous Wave (CW) operation include Free Electron Lasers, Quantum Cascade Lasers, Gunn and IMPATT diode oscillators, (typically GHz sources with Schottky diode frequency multipliers), semiconductor HBTs, HEMTs, and possibly nanometric scale silicon FETs. Table I presents a comparison of the various CW sources.

The Free Electron Laser (FEL) is in a class by itself in terms of output power (and physical size). In the FEL, electrons not bound to atoms are accelerated to relativistic speeds, then run through a "wiggler" where they give up energy which is converted to light.[5] This is shown schematically in Figure 5. Terahertz beam power in the FEL is on the order of hundreds of watts to, potentially, kilowatts. Excepting the FEL, terahertz source power is quite low, at most on the order of hundreds of milliwatts. This "terahertz gap" though narrowing, is illustrated in Figure 6.

Optically pumped lasers typically consist of a low pressure molecular gas laser pumped by a grating tuned CO_2 optical laser.[6] Output powers range from milliwatts to hundreds of milliwatts over a range of several terahertz. Quantum Cascade Lasers (QCLs) consist of a stack of repeated identical quantum well modules (typically 20–200) in which photons are created via intersubband transitions within the conduction band. QCLs have high quantum efficiency due to the cascading effect. Output power is typically in the range of tens to hundreds of milliwatts.[7–9] While not yet capable of room temperature operation, recent devices have been demonstrated at close to 140 K.

The operation of Gunn and IMPATT diodes as microwave emitters is based on these devices exhibiting regions of negative differential resistance. Small fluctuations in voltage when biased to operate in these regions tend to grow, resulting in oscillation. Simulations of GaN IMPATT diodes operating in the frequency range up to 0.7 THz have been reported recently.[10] More typically, these devices are coupled with Schottky diode frequency multipliers to achieve terahertz emission.[11] A drawback

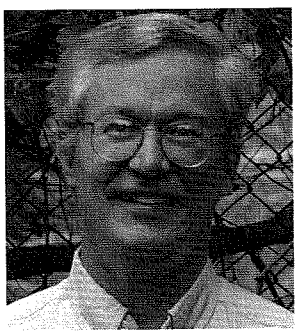

William Stillman received his M.S.E.E. in 1991 from Rensselaer Polytechnic Institute in Troy, NY. He has worked at International Business Machines since 1982, in various positions including quality assurance, failure analysis, in-line electrical test and yield diagnostics. He is presently an IGERT fellow working towards completion of his Ph.D. in electrical engineering at RPI while on educational leave from IBM. The focus of his research is on silicon FETs as detectors of terahertz and sub-terahertz radiation, and on application of terahertz radiation to testing of silicon VLSI circuits.

Michael Shur received his M.S.E.E. degree (with honors) from St. Petersburg Electrotechnical Institute, and Ph.D. and Doctor of Science degrees from A.F. Ioffe Institute. He has held positions at Ioffe, Cornell, Oakland University, University of Minnesota, and University of Virginia, where he was John Money Professor and served as Director of Applied Electrophysics Laboratories. He is now Patricia W. and C. Sheldon Roberts'48 Professor of ECSE, Professor of Physics, and Acting Director of Center for Integrated Electronics, Director of the Broadband Center, and co- Director of the NSF I/UCR Center "Connection One." Dr. Shur is a Fellow of IEEE, APS, ECS, WIF, AAAS, and EIT, Life Member of IEEE MTT, Sigma Xi, and of Humboldt Society of America, Member of Eta Kappa Nu, and Tau Beta Pi, Electromagnetic Academy, MRS, and ASEE, an Elected Member and former Chair of US Commission and elected Member of NRC of URSI (2003–2004). Dr. Shur is Editor-in-Chief of the International Journal of High Speed Electronics and Systems and of the related book series, Regional Editor of physica status solidi, and Vice-President for publications of the IEEE Sensors Council. Several of Dr. Shur's publications received the best paper awards. Among his other awards are 2007 IEEE Donald Fink Prize, 2007 IEEE Leon K. Kirchmayer Award, an Honorary Doctorate, the Gold Medal of the Russian Ministry of Education, van der Ziel Award, Senior Humboldt Research Award, Pioneer Award from Compound Semi, RPI School of Engineering Research Award, and Commendation for Excellence in Technical Communications. Dr. Shur is listed by the Institute of Scientific Information (ISI) as one of the Highly Cited Researchers. Dr. Shur is co-founder of Sensor Electronics Technology, Inc—the first commercial supplier of deep UV LEDs and the winner of the Palmetto Pillar Award for Technology Development.

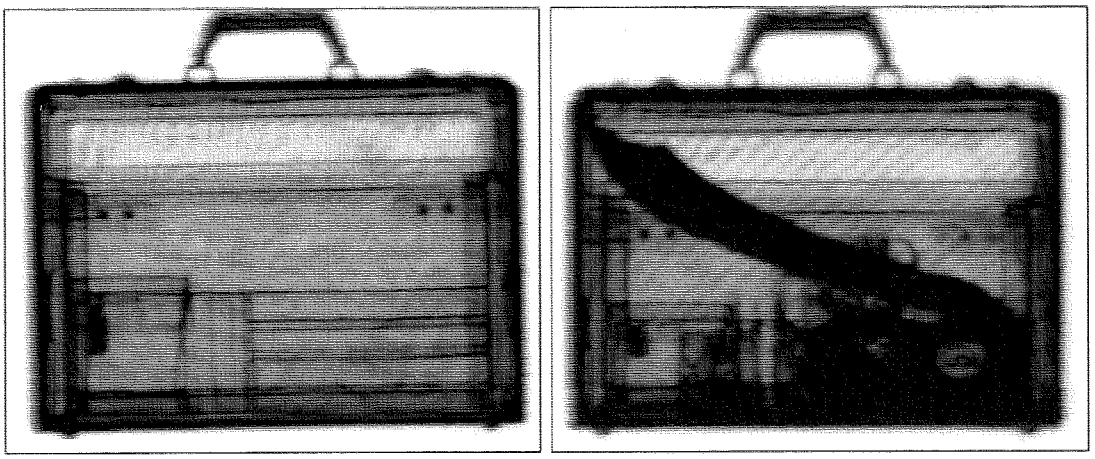

Fig. 1. 0.2 THz (active) images of empty briefcase (left) and briefcase containing a large knife and various harmless objects. Reprinted with permission from [51], N. Karpowicz et al., *Appl. Phys. Lett.* 86, 054105 **(2005)**. © 2005, American Institute of Physics.

to this approach is the reduction in emitted power with each multiplication, and power output is limited by both the power output of the source oscillator and the thermal power capacity of the multiplier. An integrated GaAs frequency doubler is shown in Figure 7.

Backward Wave Oscillators (BWOs), also known as Carcinotrons, are a variety of traveling wave tube, where energy from an electron beam traveling the length of an evacuated tube in a high magnetic field is absorbed into a waveguide intersecting the tube at regular intervals, as is shown in Figure 8. The frequency of the waveguide output is adjusted by the electron beam accelerating potential. As with Gunn and IMPATT diode sources, BWOs are often coupled to multipliers to extend their frequency.

Photomixers typically consist of an interdigitated antenna structure across which a DC bias is applied. Terahertz radiation at the difference frequency of two incident optical lasers arises from the photoelectric effect, and generally the radiation is coupled to free space using planar antennas and a hemispherical silicon lens.[12] Power output is limited by the thermal capacity of the device. Figure 9 illustrates typical photomixer structure and a commercially available packaged device.

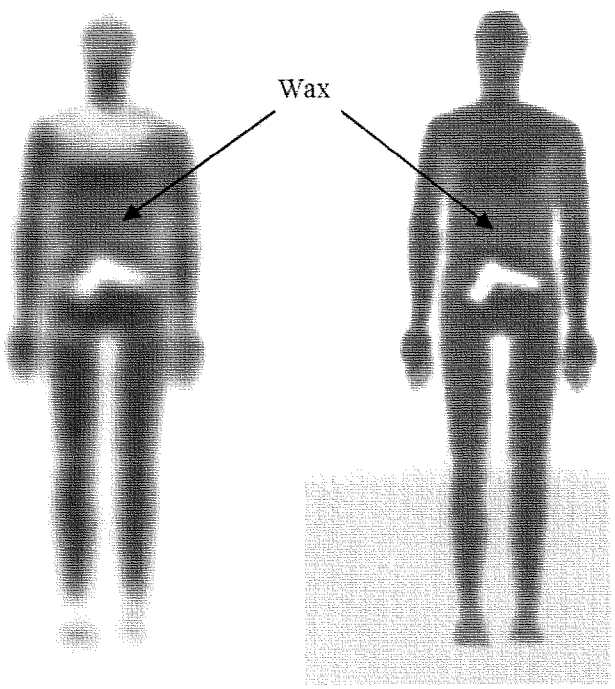

Fig. 2. Polarimetric millimeter wave scene simulations of 0.22 THz (left) and 0.50 THz (passive) images of a wax slab and metal pistol against the body. Reprinted with permission from [3], N. A. Salmon, *Proceedings of SPIE—The International Society for Optical Engineering*, London, United Kingdom **(2004)**, Vol. 5619, p. 129. © 2004, SPIE.

3. TERAHERTZ DETECTORS

In PTD systems, detection of terahertz radiation is typically accomplished using a non-linear electro-optical crystal in which the polarization of a probe beam is altered by the electric field of a present terahertz signal. For CW systems, two primary modalities exist for detection of signals in the terahertz range. One involves the reduction of the terahertz signal to sufficiently low frequencies to allow amplification and signal processing. This (heterodyne receiver) approach typically uses non-linear diodes to mix the terahertz signal with a local oscillator reference.[11] The second approach is direct detection, where the terahertz signal impinging upon a detecting device results in a measurable response. Direct detection devices include bolometers and microbolometers, Golay cells, Superconducting Tunneling Junctions (STJs), pyroelectric devices and semiconductor electronic devices including Schottky diodes, Heterojunction Bipolar Transistors (HBTs), High Electron Mobility Transistors (HEMTs) and Silicon FETs.

Among key parameters indicative of detector performance are responsivity, sensitivity (or detectivity) and response time. Responsivity relates the detector output signal to incident power, thus a more responsive detector would have a greater output (i.e., voltage) for a given

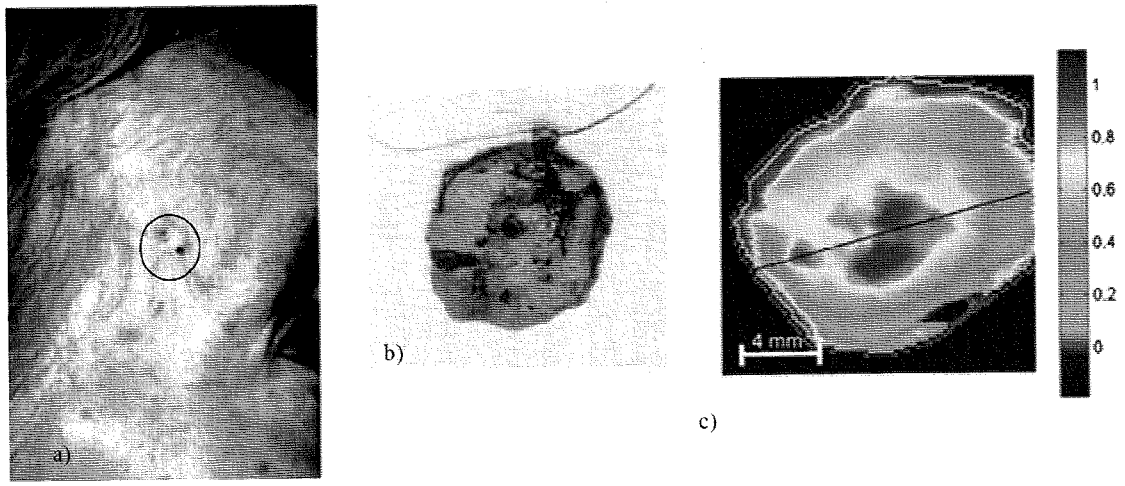

Fig. 3. *Ex-vivo* study of basal cell carcinoma: (a) clinical photograph, (b) excised tissue, (c) pulsed THz image—central dark area shows regions of increased absorption which correspond to regions of tumor. Reprinted with permission from [52], V. P. Wallace et al., *Proceedings of SPIE—The Int. Soc. for Optical Eng.*, San Jose, CA, United States **(2003)**, Vol. 4949, p. 353. © 2003, SPIE.

incident power. Sensitivity infers the minimum incident power which can be detected. Terahertz power arriving at the detector is diminished significantly by distance due to absorbtion in the atmosphere and in transmission through, or reflection from the imaged object. Additionally, ambient radiation and variations in the radiation emission process, described as radiometric fluctuation noise, place constraints upon detector sensitivity.[3]

Noise Equivalent Power (NEP) is a widely used measure inverse to sensitivity, and is frequently considered to be the minimum power detectable per square root of bandwidth, in units of W/$\sqrt{}$Hz. Useful imaging relies on the ability to differentiate materials based upon differences in power arriving at the detector. In order to realize an effective imaging system, some manner of signal or image processing will doubtless be required, for which detector response speed is of critical concern. Table II presents a comparison of NEP, responsivity, response time and operating temperature for several of the various CW detectors.

In bolometric devices, absorbed radiation changes the resistance of the detection element by increasing its temperature. These devices are extremely sensitive, due to operation cryogenic temperatures (~4 K and below), but are relatively slow in response, (recent microbolometers showing sub microsecond response[13]). Figure 10 illustrates a typical bolometer system. Detection in STJs is expected to be the result of terahertz phonons breaking Cooper pairs in the base superconducting electrode.[14]

For many emerging applications, room temperature operation is required, and among such detectors are Golay cells, pyroelectric devices, Schottky diodes, and emerging FET devices based on electron plasma waves. In Golay cells, the temperature increase due to radiation absorbtion is measured by deflection of light from a metal film deformed by an increased gas volume in the cell. Golay cells operate regardless of ambient temperature,

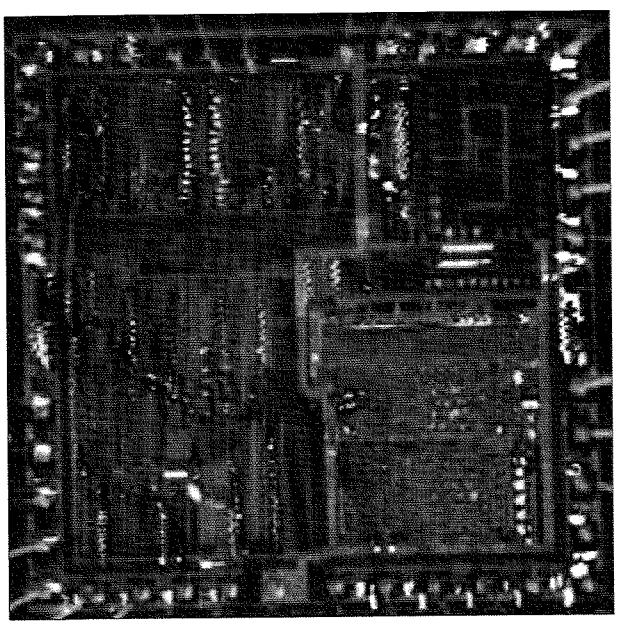

Fig. 4. THz emission image of an LSI microprocessor superimposed on its optical image. Reprinted with permission from [53], Kawase, *Optics & Photonics News* **(2004)**. © 2004, Optical Society of America.

Table I. Comparison of continuous wave terahertz sources.

	Frequency range (THz)	Output power (W)
Free electron laser[35]	0.1–10	10^{1}–10^{2}
Optically pumped IR lasers[36]	1.0–4.0	10^{-1}–10^{-3}
Quantum cascade lasers[7, 8, 37]	2.9–4.5	10^{-3}–10^{-5}
Gunn diode oscillators[38]	0.03–0.3	10^{-1}–10^{-3}
IMPATT diode oscillators[38]	0.03–0.4	10^{0}–10^{-4}
Backward wave oscillators[39, 40]	0.2–0.6	10^{-2}–10^{-3}
Frequency multipliers[11]	0.1–1.7	10^{-1}–10^{-7}
Photomixers[41, 42]	0.1–1.6	10^{-5}–10^{-7}

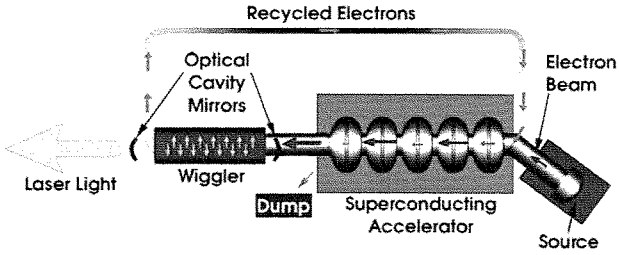

Fig. 5. Schematic illustration of light generation in a free electron laser. Electrons with unspent energy exiting the wiggler are recycled. Reprinted with permission from [35], http://www.jlab.org/FEL/ (**2007**). © 2007, Thomas Jefferson National Accelerator Facility.

but they are slow in response, and also very delicate. Figure 11 illustrates a typical Golay cell with support electronics.

Figure 12 shows a pair of typical pyroelectric detectors. In these devices, temperature changes alter the electrical polarization of the constituent materials, resulting in a voltage difference across the device terminals. Response times are on the order of milliseconds, but pyroelectric detectors are far less responsive compared with bolometric devices and Golay cells. Kachorovskii and Shur present novel pyroelectric/semiconductor systems in which polarization is accomplished via electron and hole moveable islands.[15] These islands would form the built-in voltage across pyroelectric grains embedded in a semiconductor matrix or semiconductor grains embedded in a pyroelectric matrix exceed the energy gap of the semiconductor, and are expected to exhibit a resonant response to terahertz radiation.

Response in semiconductor electronic devices is extremely fast, as might be expected given the common availability of high performance electronic goods. In Schottky diodes, response to terahertz radiation is due to rectification of the incident signal. These devices do not

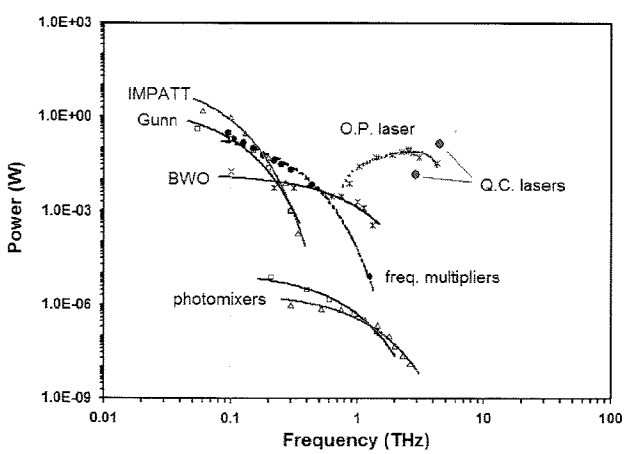

Fig. 6. Power output versus frequency of available continuous wave (CW) terahertz and sub-terahertz sources. References: IMPATT, Gunn oscillators,[38] BWO,[54] frequency multipliers,[11] photomixers,[41,42] OP laser[36] and QC lasers.[8,37]

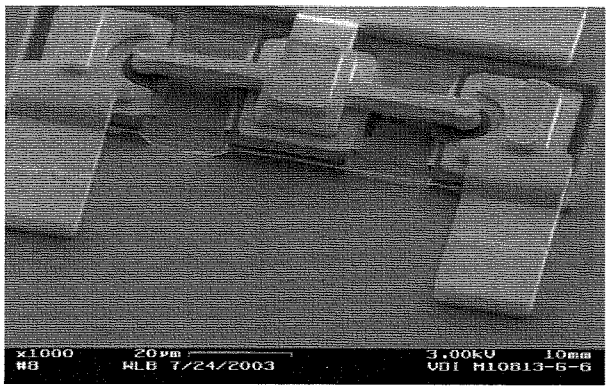

Fig. 7. SEM micrograph of an integrated GaAs Schottky diode balanced doubler to 600 GHz. Note the air bridged anode fingers between the three GaAs mesas. Reprinted with permission from [11], T. W. Crowe et al., *Proceedings of SPIE—The International Society for Optical Engineering*, Orlando, FL, United States (**2005**), Vol. 5790, p. 291. © 2005, SPIE.

suffer from carrier recombination related recovery delays, and so easily operate in the sub-terahertz range. Figure 13 shows a Schottky diode assembly for detection over the range of 0.33 to 0.50 THz. HBTs and HEMTs are also capable of operation in the sub-terahertz region.[16]

4. PLASMA WAVE PHYSICS

In 1993, Dyakonov and Shur predicted an instability of electron plasma waves in a short channel FET at terahertz frequencies.[17] As gate lengths in HEMTs and silicon MOSFETs are made increasingly smaller, charge transport becomes ballistic, and device channels behave as resonators. Terahertz response in these devices results from plasma waves being generated in the device channel due to modulation of the electron concentration. A localized decrease in electron concentration causes an excess of positive charge, attracting electrons in the vicinity. These electrons rush towards the positive charge, but because of their inertia, overshoot the charge location. Now attracted in the opposite direction, they again rush in and overshoot the charge location, hence, supporting oscillations of the electron density (i.e., plasma waves). Figure 14 compares plasma wave and transit mode performance for silicon, GaAs and GaN semiconductors.

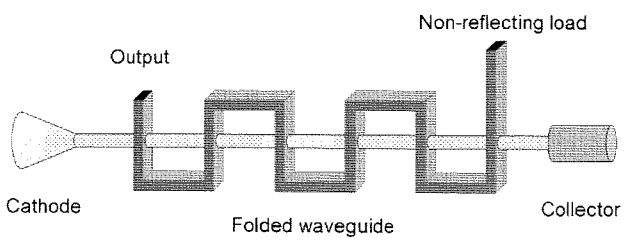

Fig. 8. Schematic diagram of a typical backward wave oscillator (after naval electrical engineering training series[55]).

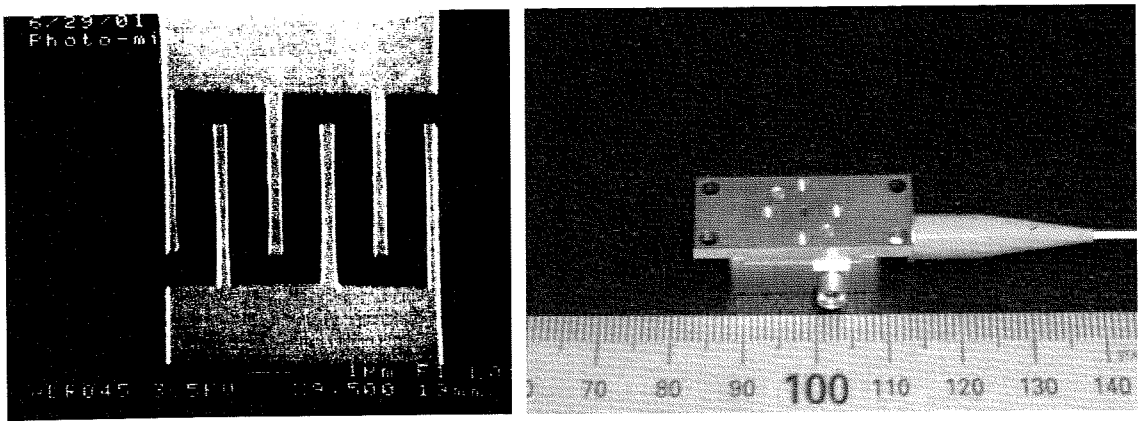

Fig. 9. (left) Micrograph of interdigitated electrode photomixer structure. Reprinted with permission from [12], E. R. Brown, *International Journal of High Speed Electronics and Systems* 13, 497 **(2003)**. © 2003, World Scientific. (right) Photograph of commercially available photomixer. Reprinted with permission from [56], A. Ueda et al., National Astronomical Observatory of Japan, Alma Memo No. 516 **(2005)**. © 2005, NAOJ.

In contemporary FETs, electron motion transverse to the channel is constrained and quantized due to high electrical fields. Charge transport is not attributed to individual carriers, but rather, to the two dimensional electron gas, which tends as a whole increasingly to conform to hydrodynamic equations of motion. Thus, as a "two dimensional electron fluid," their properties can be studied and modeled.[17] Figure 15 illustrates the plasma frequency dependencies in the 3D, ungated 2D and gated 2D regions.

Dyakonov and Shur applied the electron fluid model to terahertz detection in HEMTs in 1996.[18] The basic equations pertaining to the electron are the relation of the surface electron concentration to the gate voltage (in the region $>\eta k_B T/e$ above the threshold), the equation of motion and the continuity equation. These are solved, with appropriate boundary conditions, to yield an expression for the constant source to drain voltage response (ΔU) as:

$$\frac{\Delta U}{U_0} = \frac{1}{4}\left(\frac{U_a}{U_0}\right)^2 f(\omega) \tag{1}$$

where U_a is the ac signal induced by the incoming radiation, and:

$$f(\omega) = 1+\beta - \frac{1+\beta\cos(2k_0' L)}{\sinh^2(k_0'' L)+\cos^2(k_0' L)} \tag{2}$$

here:

$$\beta = \frac{2\omega\tau}{\sqrt{1+(\omega\tau)^2}} \tag{3}$$

and:

$$k_0' = \frac{\omega}{s}\left(\frac{\left(1+\omega^{-2}\tau^{-2}\right)^{1/2}+1}{2}\right)^{1/2} \tag{4}$$

$$k_0'' = \frac{\omega}{s}\left(\frac{\left(1+\omega^{-2}\tau^{-2}\right)^{1/2}-1}{2}\right)^{1/2} \tag{5}$$

where τ is the momentum relaxation time and $s = (eU_0/m)^{1/2}$ is the plasma wave velocity. Plasma wave devices may behave as resonant or broadband (non-resonant) detectors, as is illustrated in Figure 16, depending upon the radiation frequency and device parameters as is discussed in the next sections.

Table II. Comparison of THz CW detectors.

	NEP (W/Hz$^{1/2}$)	Responsivity (V/W)	Resp. Time (sec)	Op. Temperature (K)
Cryogenic detectors				
Bolometers[43,44]	10^{-16}–10^{-13}	10^{7}–10^{5}	10^{-2}–10^{-3}	≤4.2
Hot-e microbolometers[13,45]	10^{-19}–10^{-17}	10^{9}	10^{-8}	≤0.3
STJ detectors[46]	10^{-16}	10^{9}	10^{-3}	≤0.8
Room Temperature detectors				
Golays cells[44]	10^{-10}	10^{5}	10^{-2}	300
Pyroelectrics[47]	10^{-10}	10^{5}	10^{-2}	240–350
Schottky diodes[48]	10^{-12}	10^{3}	10^{-12}	10–420
**HEMTs[49]	10^{-10}	10^{3}	10^{-10} (Ref. [31])	10–420
**Silicon FETs[50]	10^{-10}	10^{2}	10^{-9} (Ref. [31])	10–420

**The last two entries represent emerging plasma wave electronic devices and the performance listed does not truly reflect their potential. The physics of their operation and predictions of their performance are given in the next sections.

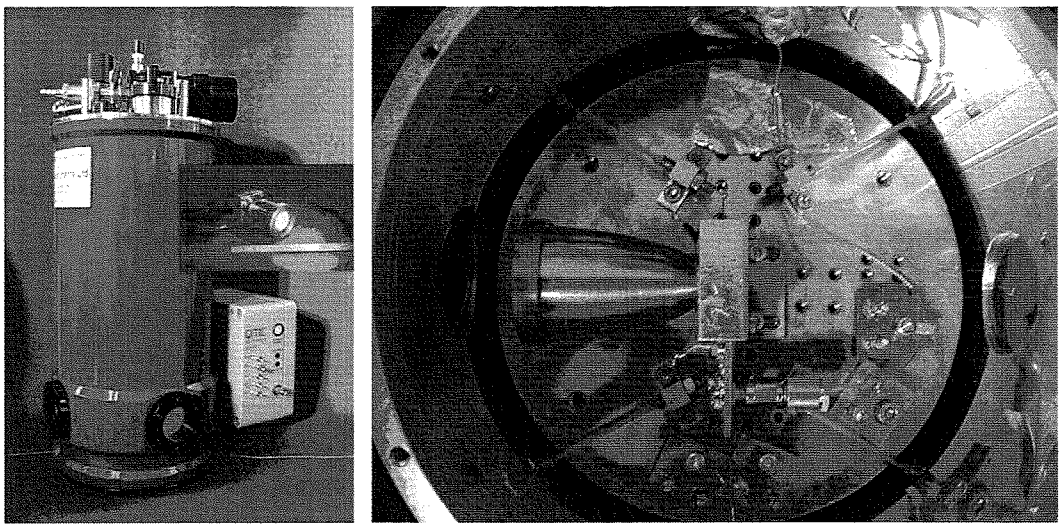

Fig. 10. (left) QNb/2 bolometer system including cryostat and support electronics. (left inset) Superconducting Nb hot electron bolometer type QNb/X, with coupling optics. (right) Internal view of cryostat illustrating bolometer placement. Reprinted with permission from [44], http://qmciworks.ph.qmw.ac.uk/QMCI/qmc.html/ **(2007)**. © 2007, QMC Instruments, Ltd.

5. NON-RESONANT DETECTION

When $\omega\tau \ll 1$, the plasma oscillations are overdamped and the device operates as a broadband detector. Here:

$$\beta \ll 1, \quad k_0' = k_0'' = (1/s)(\omega/2\tau)^{1/2} \tag{6}$$

and:

$$f(\omega) = \frac{\sinh^2(Q) - \sin^2(Q)}{\sinh^2(Q) + \cos^2(Q)} \tag{7}$$

where $Q = (L/s)(\omega/2\tau)^{1/2}$. Knap et al. extended this non-resonant response model to the sub-threshold region,[19] resulting in the expression:

$$\Delta u = \frac{eu_a^2}{4ms^2}\{(1/1 + \kappa\exp(-eU_0/\eta k_B T)) - (1/[1 + \kappa\exp(-eU_0/\eta k_B T)]^2 \times [\sinh^2(Q) + \cos^2(Q)])\} \tag{8}$$

here the plasma wave velocity s is described by:

$$s^2 = s_0^2\left[1 + \exp\left(-\frac{eU_0}{\eta k_B T}\right)\right]\ln\left[1 + \exp\left(\frac{eU_0}{\eta k_B T}\right)\right] \tag{9}$$

where $s_0 = (\eta k_B T/m)^{1/2}$ is the electron thermal velocity, and κ is a factor related to gate leakage:

$$\kappa = \frac{j_0 L^2 me}{2C\tau\eta^2 k_B^2 T^2} \tag{10}$$

where j_0 is the leakage current density and C is the gate capacitance per unit area. Calculated response of GaAs/AlGaAs FETs at 0.6 THz is shown in Figure 17. It is noted that at values well below the threshold, where the total number of electrons in the channel becomes small (gate voltage below threshold by $\ll -\alpha\eta k_B T$, where

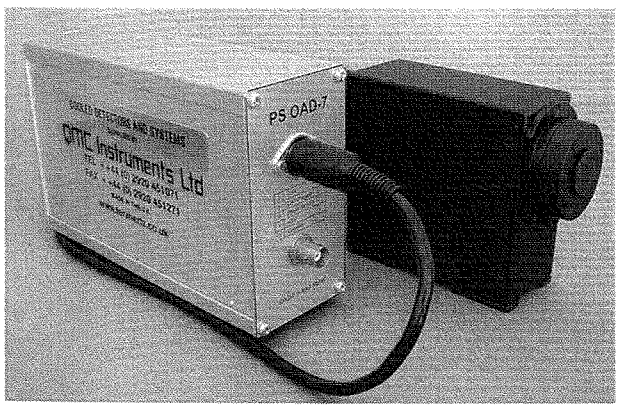

Fig. 11. Golay cell (right) and support electronics. Reprinted with permission from [44], http://qmciworks.ph.qmw.ac.uk/QMCI/qmc.html/ **(2007)**. © 2007, QMC Instruments, Ltd.

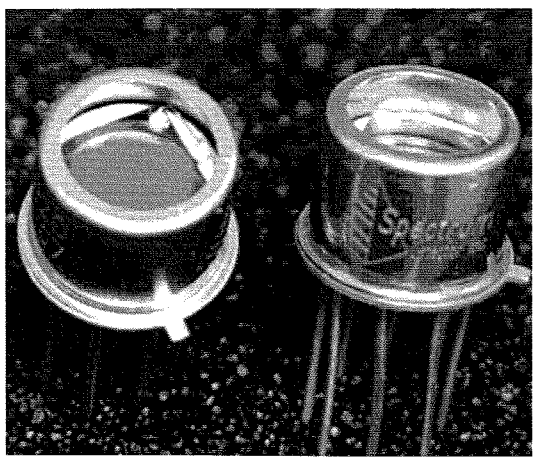

Fig. 12. $LiTaO_3$ Pyroelectric detector assemblies, available with and without integrated FET or op-amp and related circuitry. Reprinted with permission from [57], http://www.spectrumdetector.com/ **(2007)**. © 2007, Spectrum Detector, Inc.

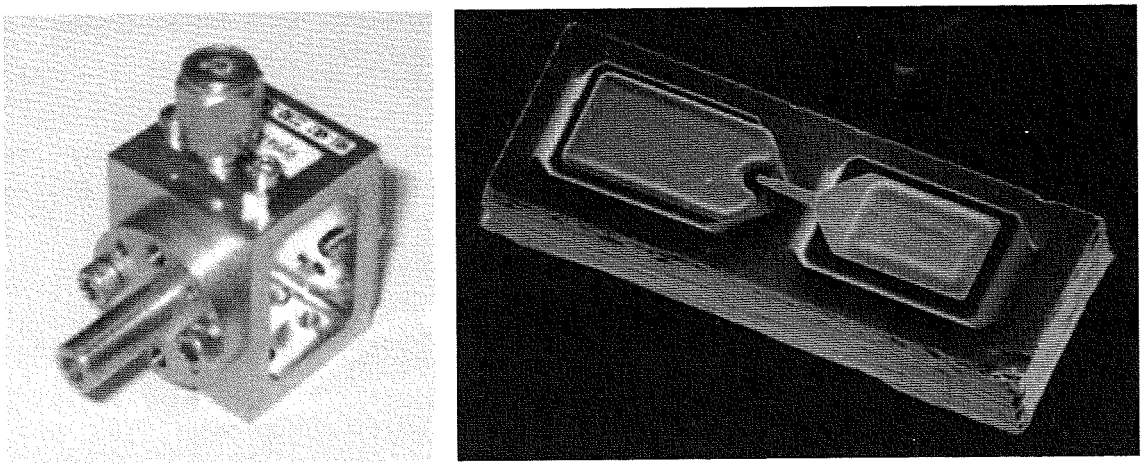

Fig. 13. (left) Zero-bias Schottky diode 0.33–0.50 THz detector assembly including feed horn assembly. Reprinted with permission from [58], http://virginiadiodes.com/ **(2007)**. © 2007, Virginia Diodes, Inc. (right) Scanning electron micrograph of a planar Schottky barrier diode. Chip dimensions are approximately $180 \times 80 \times 40$ μm. Courtesy of J. L. Hesler **(2007)**. © 2007, Virginia Diodes, Inc.

$\alpha \sim 5$ to 10), noise is found to be very important, and the model is no longer valid.

In addition to the HEMT devices studied by Knap et al., this general model has been applied to non-resonant terahertz response in submicron and nanoscale silicon MOSFETs[20, 21] and to Silicon on Insulator (SOI) MOSFETs.[22] In our recent papers, we presented the effect of device loading on sub-threshold response, and conclude that minimum detector NEP coincides with the device threshold voltage,[23] and for the first time, demonstrate non-resonant terahertz response in silicon CMOS, i.e., n-channel and p-channel devices.[24]

6. DRAIN CURRENT RESPONSE ENHANCEMENT

Lu and Shur proposed and demonstrated the increase of non-resonant response with the application of source to drain current due to increased asymmetry in plasma wave boundary conditions.[25] Veksler et al. attribute the dramatic increase in non-resonant response to the increase in non-uniformity of the electron concentration and field distributions at the transition from the linear to saturation regions.[26] They describe the detector response for long samples as follows:

$$\Delta u = \frac{u_a^2}{4U_0} \frac{1}{\sqrt{1-\lambda}} \tag{11}$$

Here λ is the ratio of the drain current density to the saturation current density j_d/j_{dsat}. As the drain current approaches the saturation current, $\lambda \to 1$, and the detector response

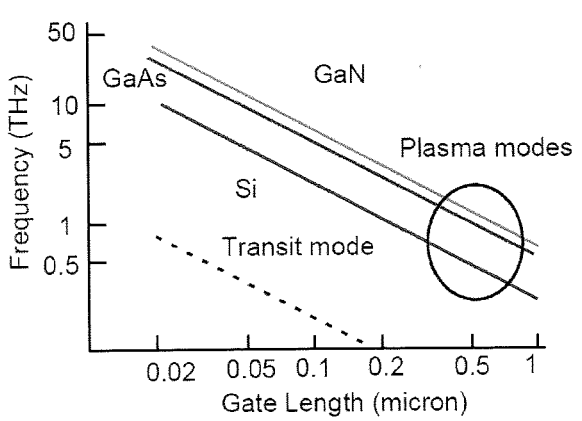

Fig. 14. Comparison of plasma and transit mode operating frequency limit versus gate length for several semiconductor materials (after Ryzhii and Shur[59]).

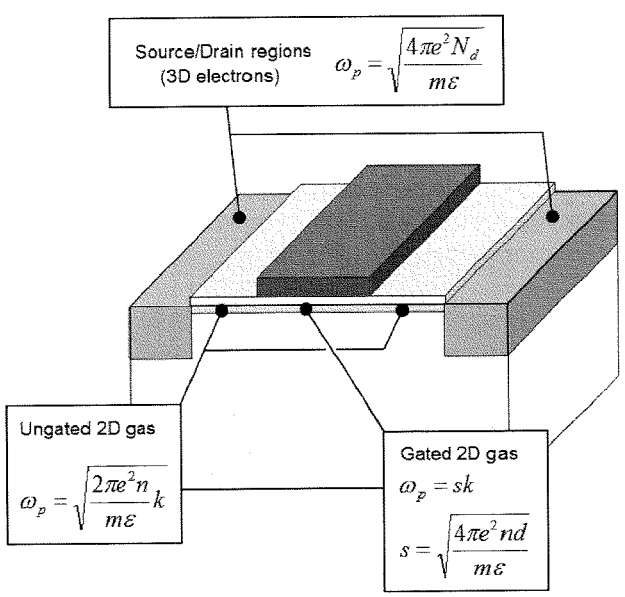

Fig. 15. Frequencies of plasma oscillations (ωp) versus wave vector (k). ε is the electron effective mass, ε is the dielectric permittivity of the semiconductor, N is the bulk electron concentration in the alloyed regions, n is the sheet electron concentration for channel regions, which is proportional to the gate voltage swing (after Shur and Ryzhii[60]).

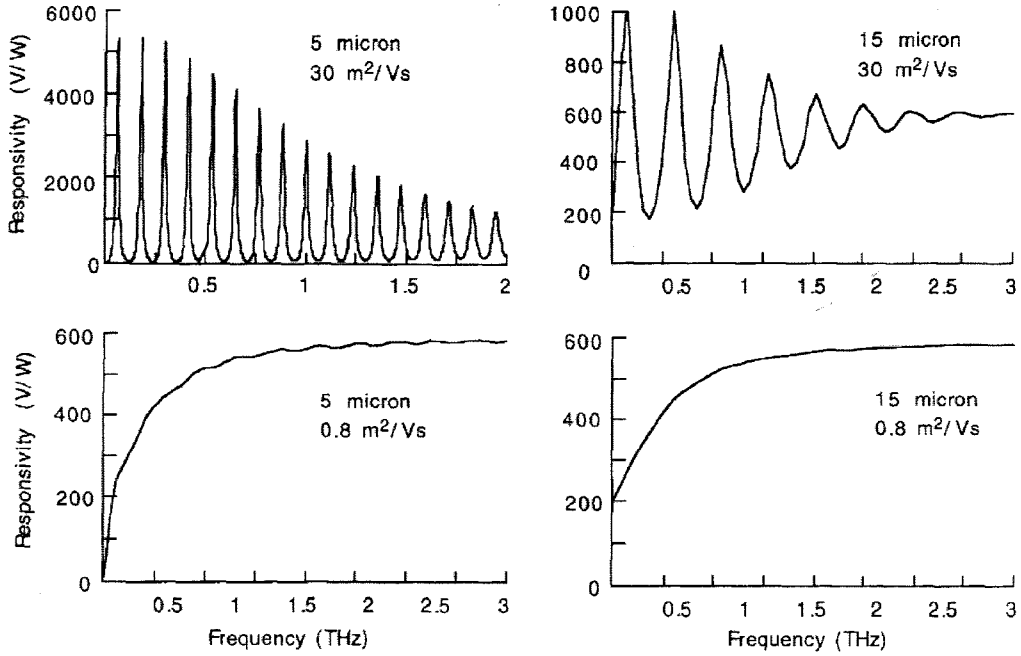

Fig. 16. Calculated responsivity of 5 μm and 15 μm gate HEMTs at 77 K (top) and 300 K (bottom). At 77 K, the devices behave as resonant detectors; at 300 K as broad-band, or non-resonant, detectors. Reprinted with permission from [61], M. I. Dya-konov and M. S. Shur, *IEEE Transactions on Electron Devices* 43, 1640 **(1996)**. © 1996, IEEE.

increases dramatically. This effect of drain current on response is illustrated in Figure 18. Teppe et al. found that the application of drain current led to an eventual transformation into resonant response in GaAs/AlGaAs FETs.[27]

7. RESONANT DETECTION

When $\omega\tau \gg 1$, the damping of the induced plasma oscillations is small. In this case:

$$\beta = 2, \quad k_0' = \frac{\omega}{s}, \quad k_0'' = (2s\tau)^{-1} \tag{12}$$

and:

$$f(\omega) = \frac{3\sinh^2(L/2s\tau) + \sin^2(\omega L/s)}{\sinh^2(L/2s\tau) + \cos^2(\omega L/s)} \tag{13}$$

For short samples where $s\tau \gg L$, $f(\omega)$ exhibits sharp resonances at the fundamental plasma frequency $\omega_0 = \pi s/2L$ and its odd harmonics. Here the response is given by:[27]

$$\Delta U \propto \frac{1}{(\omega - \omega_0)^2 + (1/2\tau)^2} \tag{14}$$

With the plasma wave bias dependent upon the gate bias, the fundamental plasma frequency is also, thus the

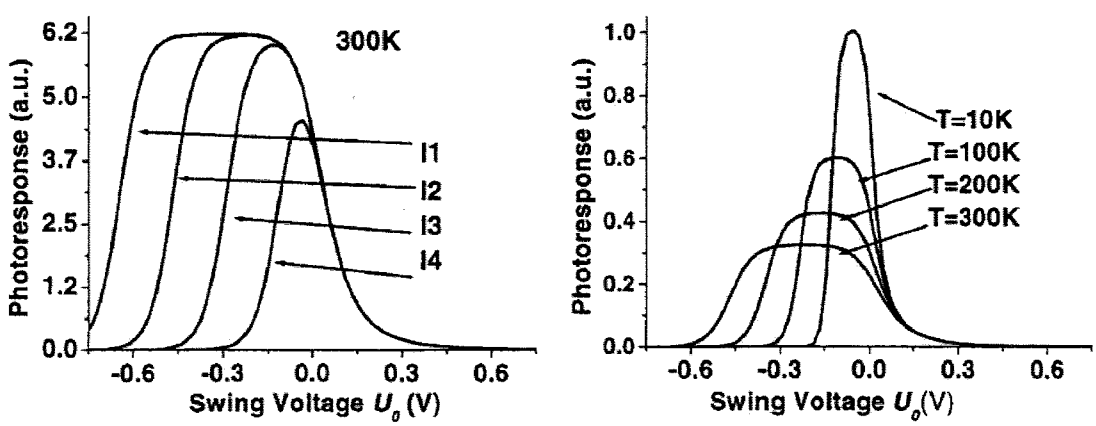

Fig. 17. Calculated GaAs/AlGaAs 0.6 THz photoresponse (left) at 300 K and for $\eta = 1.5$, for four different leakage currents. I1: $j_0 = 1.3 \times 10^1$ A/m^2, $\kappa = 10^{-7}$; I2: $j_0 = 1.3 \times 10^3$ A/m^2, $\kappa = 10^{-5}$; I3: $j_0 = 1.3 \times 10^5$ A/m^2, $\kappa = 10^{-3}$; I4: $j_0 = 1.3 \times 10^7$ A/m^2, $\kappa = 10^{-3}$, (right) at $j_0 = 1.3 \times 10^3$ A/m^2 and at four different temperatures: $T = 10$ K, $\eta = 15$, $\kappa = 9.0 \times 10^{-5}$; $T = 100$ K, $\eta = 2.5$, $\kappa = 3.2 \times 10^{-5}$; $T = 200$ K, $\kappa = 1.75$, $\kappa = 1.7 \times 10^{-5}$; $T = 300$ K, $\eta = 1.5$, $\kappa = 1.0 \times 10^{-5}$. Reprinted with permission from [19], W. Knap et al., *J. Appl. Phys.* 91, 9346 **(2002)**. © 2002, American Institute of Physics.

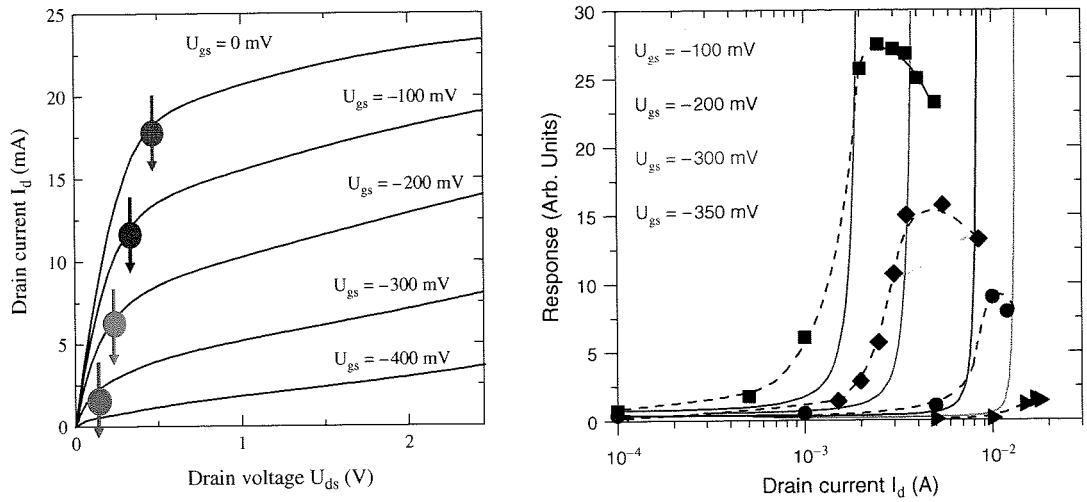

Fig. 18. (left) $I_d - V_{ds}$ characteristics of GaAs HFET. (right) Photoresponse to 0.2 THz radiation as a function of drain current (filled symbols); solid lines on right indicate theoretical predictions corresponding with the transition from linear to saturation regimes marked on $I_d - V_{ds}$ curves. Reprinted with permission from [26], D. Veksler et al., *Phys. Rev. B (Condensed Matter and Materials Physics)* 73, 125328 (http://link.aps.org/abstract/PRB/v73/p125328) **(2006)**. © 2006, American Physical Society.

device operates as a *tunable* resonant terahertz detector. Such detectors have the potential for analyzing spectral information of incoming radiation in addition to intensity. Resonant terahertz response has been demonstrated in submicron GaAs FETs[28] and in InGaP/InGaAs/GaAs HEMTs,[29] and predicted in nanometric scale silicon FETs.[21] In the absence of a developed theory of plasma waves in the saturation regime, Teppe et al. presented a "very rough" estimate of the relation between the gate bias and fundamental plasma frequency:[27]

$$\omega_0 = \frac{\pi}{2L}\sqrt{\frac{e\left(U_g' - \alpha U_{sat}\right)}{m}} \tag{15}$$

where:

$$U_g' = U_g - I_d R_s \tag{16}$$

To account for the effect of the source series resistance and α is a fitting parameter (~0.8) found experimentally. Figure 19 shows the measured and calculated resonant responses in saturation. Veksler et al. predict the decrease in resonant response width as a result of applied drain current, ultimately to zero coincident with the threshold current for plasma wave generation.[26] The resonant detector response with added drain current is expressed as:

$$\Delta U_0(L) \approx \frac{U_a^2}{4U_g}\frac{\omega_0^2}{\left(\omega - \omega_0\right)^2 + \left(1/2\tau - v_d/L\right)^2} \tag{17}$$

where v_d is the electron velocity at the drain. The width of the resonant peak is:

$$\frac{1}{2\tau_{eff}} = \frac{1}{2\tau} - \frac{v_d}{L} \tag{18}$$

Since $v_d \sim j_d$, where $j_d = |I_d|/W$ is the absolute value of the drain current density, the width of the resonant peak decreases with the drain current. Note that the response peak is not as sharp as was calculated in Figure 16. One possible reason is the presence of oblique plasma waves in the device channel, for which the resonant path length is longer than for waves traveling parallel to the device channel length.[30]

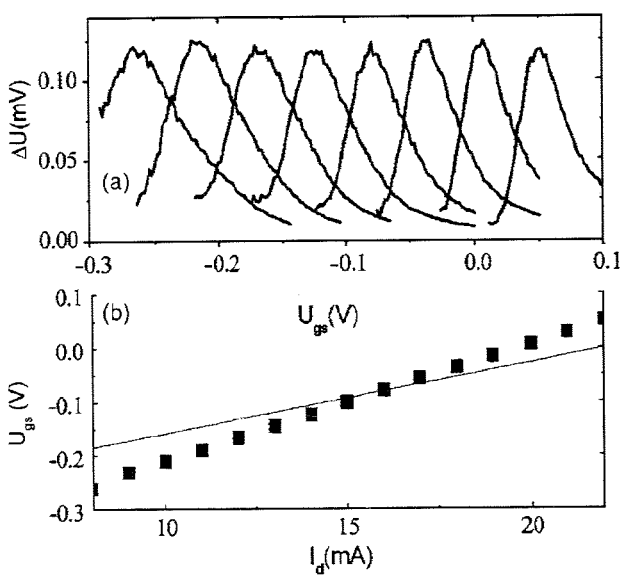

Fig. 19. (top) 0.6 THz response as a function of gate voltage for drain currents from 8 mA to 22 mA (left to right) in 2 mA steps. (bottom) Position of the response maxima versus applied drain current (squares) and calculated dependence (solid line). Reprinted with permission from [27], F. Teppe et al., *Appl. Phys. Lett.* 87, 052107 **(2005)**. © 2005, American Institute of Physics.

8. RESPONSE SPEED

Detector response speed is of great importance in sensing applications involving substantial image processing. Kachorovskii and Shur have recently proposed theoretical calculation of the maximum response modulation frequency in plasma wave detectors as shown in the following expression.[31]

$$f_{\max} = \begin{cases} \dfrac{\mu U_0}{2\pi L^2} & U_0 > 0, \quad eU_0 \gg T \\ \dfrac{\mu \eta k_B T}{2\pi e L^2} & U_0 < 0, \quad e|U_0| \gg T \end{cases} \tag{19}$$

Near $U_0 = 0$, $f_{\max}$ is interpolated as:

$$f_{\max} = \left(\frac{\mu \eta k_B T}{2\pi e L^2}\right)\left[1 + \exp\left(\frac{-eU_0}{\eta k_B T}\right)\right] \times \ln\left[1 + \exp\left(\frac{eU_0}{\eta k_B T}\right)\right] \tag{20}$$

For gate lengths of 200 nm, estimates of $f_{\max}$ at the device threshold are 10 GHz and 75 GHz for silicon and GaAs, respectively, as is shown in Figure 20. Due to the strong dependence on channel length ($1/L^2$), $f_{\max}$ is increased dramatically as devices become shorter; for example, in silicon devices with contemporary gate lengths of ~50 nm, $f_{\max}$ increases to more than 20 GHz at the device threshold.

9. PLASMA WAVE EMITTERS

The possibility of realizing an electronic terahertz oscillator based on electron plasma waves was first presented by Dyakonov and Shur in 1993.[17] Here, the ballistic FET is expected to perform as a point or linear source of

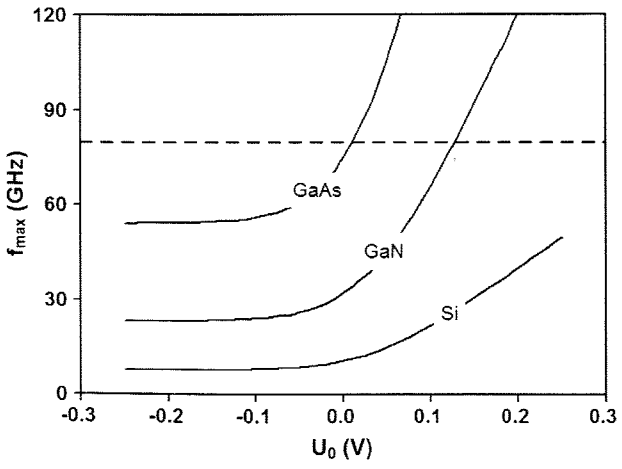

Fig. 20. Dependence of $f_{\max}$ on gate bias for several semiconductor materials at room temperature with $L = 200$ nm. Typical values of mobility were used for GaAs (3500 cm²/Vs), GaN (1500 cm²/Vs) and silicon (500 cm²/Vs). The dashed line corresponds to velocity saturation with $f_{\max} = v_s/2\pi L$ where $v_s = 1 \times 10^7$ cm/s (after Kachorovskii and Shur[31]).

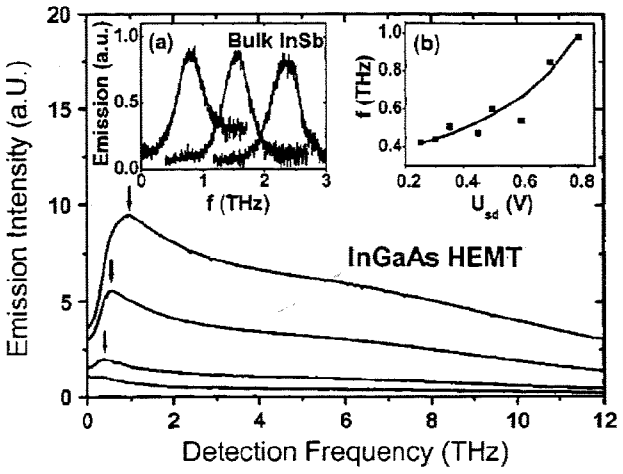

Fig. 21. Emission spectra from InGaAs/AlInAs HEMTs at 4.2 K. Inset (a) emission spectra of bulk InSb during system calibration. Inset (b) resonant frequency dependence of HEMT emission versus gate bias. Reprinted with permission from [33], W. Knap et al., *Appl. Phys. Lett.* 84, 2331 (**2004**). © 2004, American Institute of Physics.

electromagnetic radiation in the terahertz range due to amplification of electron plasma waves during reflection from the fixed current boundary. Deng et al. were the first to observe sub-terahertz emission from GaN/AlGaN HEMTs at cryogenic temperatures.[32] Terahertz emission was demonstrated in 60 nm gate length InGaAs/AlInAs HEMTs at cryogenic temperature (4.2 K) in 2004 by Knap et al.[33] Figure 21 illustrates the emission spectra of and resonant frequency dependence upon the gate bias. Room temperature emission was demonstrated by Dyakonova et al. in 2006.[34] Figure 22 compares the measured response at 4.2 K and 300 K.

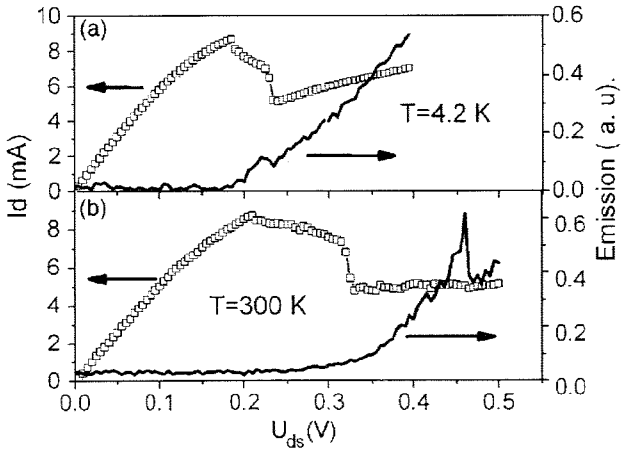

Fig. 22. Current–voltage characteristics (left axis) and emission intensities (right axis) for InAlAs/InGaAs HEMTs at 4.2 K (top) and 300 K (bottom). Note sub-threshold appearance of emission intensity coincident with downward transition in drain current. Reprinted with permission from [34], N. Dyakonova et al., *Appl. Phys. Lett.* 88, 141906 (**2006**). © 2006, American Institute of Physics.

REVIEW

10. CONCLUSIONS

As terahertz applications emerge, the need for sensitive detectors capable of fast response and room temperature operation is becoming increasingly apparent. Plasma wave devices, presently being researched, offer performance comparable to commercially available devices with the advantages of very fast response speed and also, very significantly, *tunable* response in devices with sufficiently high carrier mobilities and short channel lengths. In addition, these resonant devices have shown promise as terahertz emitters.

Acknowledgments: W. J. Stillman is supported by the NSF (Grant No. 0333314), and by the NSF Connection One I/UCRC at RPI.

References and Notes

1. R. Bogue, *Sensor Review* 25, 123 (**2005**).
2. N. Karpowicz, H. Zhong, J. Xu, K.-I. Lin, J.-S. Hwang, and X. C. Zhang, *Semicond. Sci. Technol.* 20, 293 (**2005**).
3. N. A. Salmon, *Proceedings of SPIE—The International Society for Optical Engineering*, United Kingdom, London (**2004**).
4. H. Hamster, A. Sullivan, S. Gordon, W. White, and R. W. Falcone, *Phys. Rev. Lett.* 71, 2725 (**1993**).
5. H. F. Dylla and S. T. Corneliussen, *Photonics Spectra* 39, 62 (**2005**).
6. Coherent - DEOS, http://www.cohr.com/downloads/OpticallyPumpedLaser.pdf (**2001**).
7. R. Kohler, A. Tredicucci, F. Beltram, H. E. Beere, E. H. Linfield, A. G. Davies, D. A. Ritchie, S. S. Dhillon, and C. Sirtori, *Appl. Phys. Lett.* 82, 1518 (**2003**).
8. B. S. Williams, Q. Qin, S. Kumar, Q. Hu, and J. L. Reno, *Proceedings of SPIE—The International Society for Optical Engineering*, San Jose, CA, United States (**2007**).
9. C. Worrall, J. Alton, M. Houghton, S. Barbieri, C. Sirtori, H. E. Beere, and D. Ritchie, *Proceedings of SPIE—The International Society for Optical Engineering*, San Jose, CA, United States (**2006**).
10. A. Reklaitis and L. Reggiani, *J. Appl. Phys.* 95, 7925 (**2004**).
11. T. W. Crowe, D. W. Porterfield, J. L. Hesler, W. L. Bishop, D. S. Kurtz, and H. Kai, *Proceedings of SPIE—The International Society for Optical Engineering*, Orlando, FL, USA (**2005**).
12. E. R. Brown, *International Journal of High Speed Electronics and Systems* 13, 497 (**2003**).
13. L. Kuzmin, M. Fominsky, A. Kalabukhov, D. Golubey, and M. Tarasov, *Proceedings of SPIE—The International Society for Optical Engineering*, Waikaloa, HI, United States (**2002**).
14. T. Taino, R. Nakano, S. Yoshimura, H. Myoren, S. Takada, C. Otani, S. Ariyoshi, T. Shibuya, K. Kawase, H. Sato, and H. M. Shimizu, *Nucl. Instrum. Methods Phys. Res., Sect. A: Accelerators, Spectrometers, Detectors and Associated Equipment* 559, 751 (**2006**).
15. V. Y. Kachorovskii and M. S. Shur, *Appl. Phys. Lett.* 86, 012101 (**2005**).
16. J.-S. Rieh, B. Jagannathan, D. R. Greenberg, M. Meghelli, A. Rylyakov, F. Guarin, Z. Yang, D. C. Ahlgren, G. Freeman, P. Cottrell, and D. Harame, *IEEE Transactions on Microwave Theory and Techniques* 52, 2390 (**2004**).
17. M. Dyakonov and M. Shur, *Phys. Rev. Lett.* 71, 2465 (**1993**).
18. M. Dyakonov and M. Shur, *IEEE Transactions on Electron Devices* 43, 380 (**1996**).
19. W. Knap, V. Kachorovskii, Y. Deng, S. Rumyantsev, J. Q. Lu, R. Gaska, M. S. Shur, G. Simin, X. Hu, M. Asif Khan, C. A. Saylor, and L. C. Brunel, *J. Appl. Phys.* 91, 9346 (**2002**).
20. W. Knap, F. Teppe, Y. Meziani, N. Dyakonova, J. Lusakowski, F. Boeuf, T. Skotnicki, D. Maude, S. Rumyantsev, and M. S. Shur, *Appl. Phys. Lett.* 85, 675 (**2004**).
21. F. Teppe, Y. M. Meziani, N. Dyakonova, J. Lusakowski, F. Boeuf, T. Skotnicki, D. Maude, S. Rumyantsev, M. S. Shur, and W. Knap, *Physica Status Solidi C: Conferences* 2, 1413 (**2005**).
22. N. Pala, F. Teppe, D. Veksler, Y. Deng, M. S. Shur, and R. Gaska, *Electron. Lett.* 41, 447 (**2005**).
23. W. Stillman, M. S. Shur, D. Veksler, S. Rumyantsev, and F. Guarin, *Electron. Lett.* 43, 422 (**2007**).
24. W. Stillman, F. Guarin, V. Y. Kachorovskii, N. Pala, S. Rumyantsev, M. S. Shur, and D. Veksler, *6th Annual IEEE Conference on Sensors*, Atlanta, GA (**2007**).
25. J. Q. Lu and M. S. Shur, *Appl. Phys. Lett.* 78, 2587 (**2001**).
26. D. Veksler, F. Teppe, A. P. Dmitriev, V. Y. Kachorovskii, W. Knap, and M. S. Shur, *Physical Review B (Condensed Matter and Materials Physics)* 73, 125328 (**2006**).
27. F. Teppe, W. Knap, D. Veksler, M. S. Shur, A. P. Dmitriev, V. Y. Kachorovskii, and S. Rumyantsev, *Appl. Phys. Lett.* 87, 052107 (**2005**).
28. W. Knap, Y. Deng, S. Rumyantsev, and M. S. Shur, *Appl. Phys. Lett.* 81, 4637 (**2002**).
29. T. Otsuji, M. Hanabe, and O. Ogawara, *Appl. Phys. Lett.* 85, 2119 (**2004**).
30. M. I. Dyakonov, private conversation (**2005**).
31. V. Y. Kachorovskii and M. S. Shur, *Solid-State Electron.* (**2007**), in press.
32. Y. Deng, R. Kersting, J. Xu, R. Ascazubi, X.-C. Zhang, M. S. Shur, R. Gaska, G. S. Simin, M. Asif Khan, and V. Ryzhii, *Appl. Phys. Lett.* 84, 70 (**2004**).
33. W. Knap, J. Lusakowski, T. Parenty, S. Bollaert, A. Cappy, V. V. Popov, and M. S. Shur, *Appl. Phys. Lett.* 84, 2331 (**2004**).
34. N. Dyakonova, A. El Fatimy, J. Lusakowski, W. Knap, M. I. Dyakonov, M. A. Poisson, E. Morvan, S. Bollaert, A. Shchepetov, Y. Roelens, C. Gaquiere, D. Theron, and A. Cappy, *Appl. Phys. Lett.* 88, 141906 (**2006**).
35. Thomas Jefferson National Accelerator Facility, http://www.jlab.org/FEL/felspecs.html (**2007**).
36. Coherent, http://www.cohr.com/downloads/SIFIR50_DSrevB.pdf (**2007**).
37. S. Barbieri, J. Alton, H. E. Beere, J. Fowler, E. H. Linfield, and D. A. Ritchie, *Appl. Phys. Lett.* 85, 1674 (**2004**).
38. G. I. Haddad, J. R. East, and H. Eisele, *International Journal of High Speed Electronics and Systems* 13, 395 (**2003**).
39. M. Y. Tretyakov, S. A. Volokhov, G. Y. Golubyatnikov, E. N. Karyakin, and A. F. Krupnov, *International Journal of Infrared and Millimeter Waves* 20, 1443 (**1999**).
40. E. A. Michael, U. U. Graf, C. E. Honingh, K. Jacobs, F. Lewen, R. Schieder, and J. Stutzki, SOFIA Terahertz Array Receiver (STAR), Munich, Germany (**2000**).
41. S. Verghese, K. A. McIntosh, and E. R. Brown, *Appl. Phys. Lett.* 71, 2743 (**1997**).
42. M. Mikulics, E. A. Michael, R. Schieder, J. Stutzki, R. Gusten, M. Marso, A. van der Hart, H. P. Bochem, H. Luth, and P. Kordos, *Appl. Phys. Lett.* 88, 41118 (**2006**).
43. P. L. Richards, *J. Appl. Phys.* 76, 1 (**1994**).
44. QMC Instruments, http://qmciworks.ph.qmw.ac.uk/QMCI/qmc.html (**2006**).
45. T. R. Stevenson, W.-T. Hsieh, R. R. Mitchell, H. D. Isenberg, C. M. Stahle, N. T. Cao, G. Schneider, D. E. Travers, S. H. Moseley, E. J. Wollack, and R. M. Henry, *Nucl. Instrum. Methods Phys. Res., Sect. A: Accelerators, Spectrometers, Detectors and Associated Equipment* 559, 591 (**2006**).

46. S. Ariyoshi, C. Otani, A. Dobroiu, H. Sato, K. Kawase, H. M. Shimizu, T. Taino, and H. Matsuo, *Appl. Phys. Lett.* 88, 203503 **(2006)**.

47. Spectrum Detector Inc., http://www.spectrumdetector.com/pdf/datasheets/THZ.pdf **(2007)**.

48. P. Chahal, F. Morris, and G. Frazier, *IEEE Electron Device Letters* 26, 894 **(2005)**.

49. A. V. Antonov, V. I. Gavrilenko, E. V. Demidov, S. V. Morozov, A. A. Dubinov, J. Lusakowski, W. Knap, N. Dyakonova, E. Kaminska, A. Piotrowska, K. Golaszewska, and M. S. Shur, *Physics of the Solid State* 46, 146 **(2004)**.

50. R. Tauk, F. Teppe, S. Boubanga, D. Coquillat, W. Knap, Y. M. Meziani, C. Gallon, F. Boeuf, T. Skotnicki, C. Fenouillet-Beranger, D. K. Maude, S. Rumyantsev, and M. S. Shur, *Appl. Phys. Lett.* 89, 253511 **(2006)**.

51. N. Karpowicz, H. Zhong, C. Zhang, K.-I. Lin, J.-S. Hwang, J. Xu, and X. C. Zhang, *Appl. Phys. Lett.* 86, 054105 **(2005)**.

52. V. P. Wallace, R. M. Woodward, A. J. Fitzgerald, E. Pickwell, R. J. Pye, and D. A. Arnone, Terahertz Pulsed Imaging of Cancers, San Jose, CA, United States **(2003)**.

53. K. Kawase, Terahertz Imaging For Drug Detection & Large-Scale Integrated Circuit Inspection, *Optics & Photonics News* **(2004)**.

54. MicroTech Instruments, http://mtinstruments.com/downloads/Microtech%20Product%20Catalog.pdf **(2007)**.

55. Integrated Publishing, http://www.tpub.com/content/neets/14183/css/14183_103.htm **(2007)**.

56. A. Ueda, Y. Sekimoto, M. Ishiguro, S. Asayama, M. Yamada, and T. Noguchi, Evaluation of a Commercially Available High Efficiency Photomixer, National Astronomical Observatory of Japan, Alma Memo No. 516 **(2005)**.

57. Spectrum Detector Inc., http://www.spectrumdetector.com/ **(2007)**.

58. http://virginiadiodes.com/ **(2007)**.

59. V. Ryzhii and M. S. Shur, *2003 International Semiconductor Device Research Symposium (IEEE Cat. No.03EX741)*, Washington, DC, USA **(2003)**.

60. M. S. Shur and V. Ryzhii, *11th GAAS Symposium*, Munich **(2003)**.

61. M. I. Dyakonov and M. S. Shur, *IEEE Transactions on Electron Devices* 43, 1640 **(1996)**.

Received: 11 October 2007. Revised/Accepted: 23 October 2007.